CrossMark

Glaciomarine sedimentation and bottom current activity on the north-western and northern continental margins of Svalbard during the late Quaternary

Teena Chauhan[1,2] · Riko Noormets[1] · Tine L. Rasmussen[2,3]

Abstract Palaeo-bottom current strength of the West Spitsbergen Current (WSC) and the influence of the Svalbard-Barents Sea Ice Sheet (SBIS) on the depositional environment along the northern Svalbard margins are poorly known. Two gravity cores from the southern Yermak Plateau and the upper slope north of Nordaustlandet, covering marine isotope stage (MIS) 1 to MIS 5, are investigated. Five lithofacies, based on grain size distribution, silt/clay ratio, content and mean of sortable silt (SS), are distinguished to characterise the contourite-dominated sedimentary environments. In addition, depositional environments are described using total organic carbon (TOC), total sulphur (TS) and calcium carbonate ($CaCO_3$) contents of sediments. Facies A, containing coarse SS, suggests strong bottom current activity and good bottom water ventilation conditions as inferred from low TOC content. This facies was deposited during the glacial periods MIS 4, MIS 2 and during the late Holocene. Facies B is dominated by fine SS indicating weak bottom current and poor ventilation (cf. high TOC content of 1.2–1.6%), and correlates with the MIS 4/3 and MIS 2/1 transition periods. With an equal amount of clay and sand, fine SS and high content of TOC, facies C indicates reduced bottom current strength for intervals with sediment supply from proximal sources such as icebergs, sea ice or meltwater discharge. This facies was

deposited during the last glacial maximum. Facies D represents mass-flow deposits on the northern Svalbard margin attributed to the SBIS advance at or near the shelf edge. Facies E sediments indicating moderate bottom current strength were deposited during MIS 5 and MIS 3, and during parts of MIS 2. This first late Quaternary proxy record of the WSC flow and sedimentation history from the northern Svalbard margin suggests that the oceanographic conditions and ice sheet processes have exerted first-order control on sediment properties.

Introduction

Contourites, or sediment deposits affected by alongside bottom currents, contain the signature of past ocean circulation and climate (Rebesco et al. 2014). Seabed sediments are well suited for the reconstruction of palaeoceanographic and climatic variability also due to their relatively continuous nature and good age control. The continental margins of high-latitude regions have received sediments from bottom currents and from external sources as well. Consequently, sediments on the upper continental slope record the interplay between sea-level changes, ice sheet dynamics on the adjacent shelf and associated sediment delivery to the shelf edge, down-slope mass transport of sediments, along-slope sweeping of contourite currents, and iceberg and sea ice processes. The West Spitsbergen Current (WSC), the northward-flowing branch of the North Atlantic Current, carries relatively warm Atlantic Water (AW) to the Arctic Ocean via the eastern Fram Strait (Rudels et al. 2012). The upper continental slope sectors northwest and north of Svalbard are located along the main route of the AW flow to the Arctic Ocean and, therefore, they are in a strategic position for recording the palaeo-bottom current activity of the WSC and its influence on the Svalbard-Barents Sea ice sheet (SBIS).

✉ Teena Chauhan
chauhan2081@gmail.com

[1] Department of Arctic Geology, The University Centre in Svalbard (UNIS), P.O. Box 156, 9171 Longyearbyen, Norway

[2] Department of Geology, UiT The Arctic University of Norway, 9037 Tromsø, Norway

[3] CAGE - Centre for Arctic Gas Hydrate, Environment and Climate, UiT The Arctic University of Norway, 9037 Tromsø, Norway

Previous studies from these areas have focused mainly on the temporal variations of water masses along the path of the WSC using micropalaeontological and stable isotope records (Wollenburg et al. 2001; Koç et al. 2002; Slubowska et al. 2005; Rasmussen et al. 2014a; Chauhan et al. 2014, 2015). Hence, the information on bottom current activity on the upper slope and shelf is mainly based on the relative abundance of the benthic foraminiferal species *Cibicides lobatulus*, an indicator of strong bottom current activity. In addition, grain size distribution is explained primarily based on the lithology and ice-rafted debris (IRD) records. Sedimentological and organo-geochemical studies have focused on the lower slope areas of the Yermak Plateau (Birgel and Hass 2004; Howe et al. 2008). along the northern Barents Sea margin (Knies and Stein 1998; Knies et al. 1999) and along the western Barents Sea margin (Lucchi et al. 2013; Jessen and Rasmussen 2015). There is a clear gap in knowledge on the physical characteristics of bottom currents and associated depositional environments in the upper slope–shelf regions of the northern Svalbard margins. Moreover, comparisons of published records based on other proxies (e.g. stable isotopes and foraminiferal fauna studies) with those based on grain size analysis to infer past bottom current activity are needed.

In this study, two cores collected on the north-western (JM10-02GC) and northern (HH11-09GC) margin of Svalbard are evaluated with the aim to reconstruct bottom current variability and the associated depositional processes. For reconstruction of bottom current activity of the WSC during the late Quaternary, the focus is on the grain size distribution of the 10–63 μm fraction, the so-called sortable silt (SS), which can be a proxy for near-bottom current strength (McCave et al. 1996; McCave and Hall 2006). Numerous studies have shown that mean SS ($\overline{SS}$) can reflect the flow strength of bottom currents (e.g. Gröger et al. 2003; Sternal et al. 2014; McCave et al. 2014). However, due to mixing of sediments from iceberg and sea ice in the study area, other parameters such as grain size distribution and silt/clay ratios are also considered in the interpretation of bottom current variability. The silt/clay ratio provides information complementary to the $\overline{SS}$ proxy; e.g. a high silt/clay ratio and a coarse $\overline{SS}$ have been shown to be indicative of relatively strong bottom currents and vice versa (Prins et al. 2002). A negative correlation between the two parameters is an indication of transport distance; in the Arctic, for example, a coarser $\overline{SS}$ and a low silt/clay ratio suggest that the coarser sediment may have been supplied from sources close to a given study site, such as nearby meltwater plumes or iceberg melt-out.

For reconstruction of the depositional environment, total organic carbon (TOC), total sulphur (TS) and calcium carbonate (CaCO_3) contents in the sediments are measured. TOC originates from marine biological productivity and/or terrestrial sources, and is a function of sedimentation rate, sediment

type and texture, and the conditions of bottom water ventilation. The major portion of organic carbon dissolves in the water column, at the sediment–water interface and within the sediment (Emerson and Hedges 1988; Canfield et al. 1993; Canfield 1994). Therefore, TOC can be used to study variations in the local bottom water ventilation, which vary with glacial-interglacial changes (Müller and Suess 1979; Hedges and Keil 1995). Other than these proxies, earlier published sedimentological and stable isotope records (Chauhan et al. 2014, 2015) are used as supportive evidence to correlate and interpret the depositional environments, bottom water ventilation and the near-bottom current strength of the WSC.

Regional setting

The Svalbard archipelago is located in the north-western part of the Barents Sea east of the Fram Strait, which is the only deep-water connection between the Arctic Ocean and the northern Atlantic Ocean (Fig. 1). During the last glacial maximum, the SBIS extended out to the shelf edge along the western and northern Svalbard margin, affecting the sedimentation and oceanographic conditions along the continental slope (Svendsen et al. 2004; Howe et al. 2008; Jessen et al. 2010). Glacial lineations on the southern Yermak Plateau have been shown to originate from marine isotope stage (MIS) 6, suggesting that this was the last time when a large ice mass (ice shelf or large icebergs) was grounded northwest of Svalbard in a water depth of ca. 600 m (Dowdeswell et al. 2010).

The modern oceanographic system influencing the north-western and northern Svalbard margins is dominated by the WSC, which transports warm and saline AW to the Arctic Ocean. Currently, in the Eurasian part of the Arctic Ocean, heat of the AW controls the formation and stability of sea ice (Rippeth et al. 2015). The AW flows northwards as a surface water mass along the western Svalbard margin and continues below the ice-covered Polar Water of the Arctic Ocean in the northern Fram Strait. At approximately 80°N, water masses shallower than 500 m deflect eastwards and flow along the northern Svalbard margin as the Svalbard Branch of the WSC (Fig. 1). The water mass below 500 m depth follows the continental slope and flows northwards up to 81°N as the Yermak Branch. At 81°N, the Yermak Branch turns east and flows around the north-western tip of the Yermak Plateau joining the Svalbard Branch (Rudels et al. 2012). Oceanographic data from the east–west oriented linear array of moorings in the eastern Fram Strait along 78°50′N yield an average northward current velocity of 20 cm/s in the upper part of the water column (Fahrbach et al. 2001; Schauer et al. 2004; Rebesco et al. 2013). Presently, the northern margin of Svalbard is covered by seasonal sea ice.

Contourites described on the western slope of the Yermak Plateau in the eastern Fram Strait suggest that contour currents
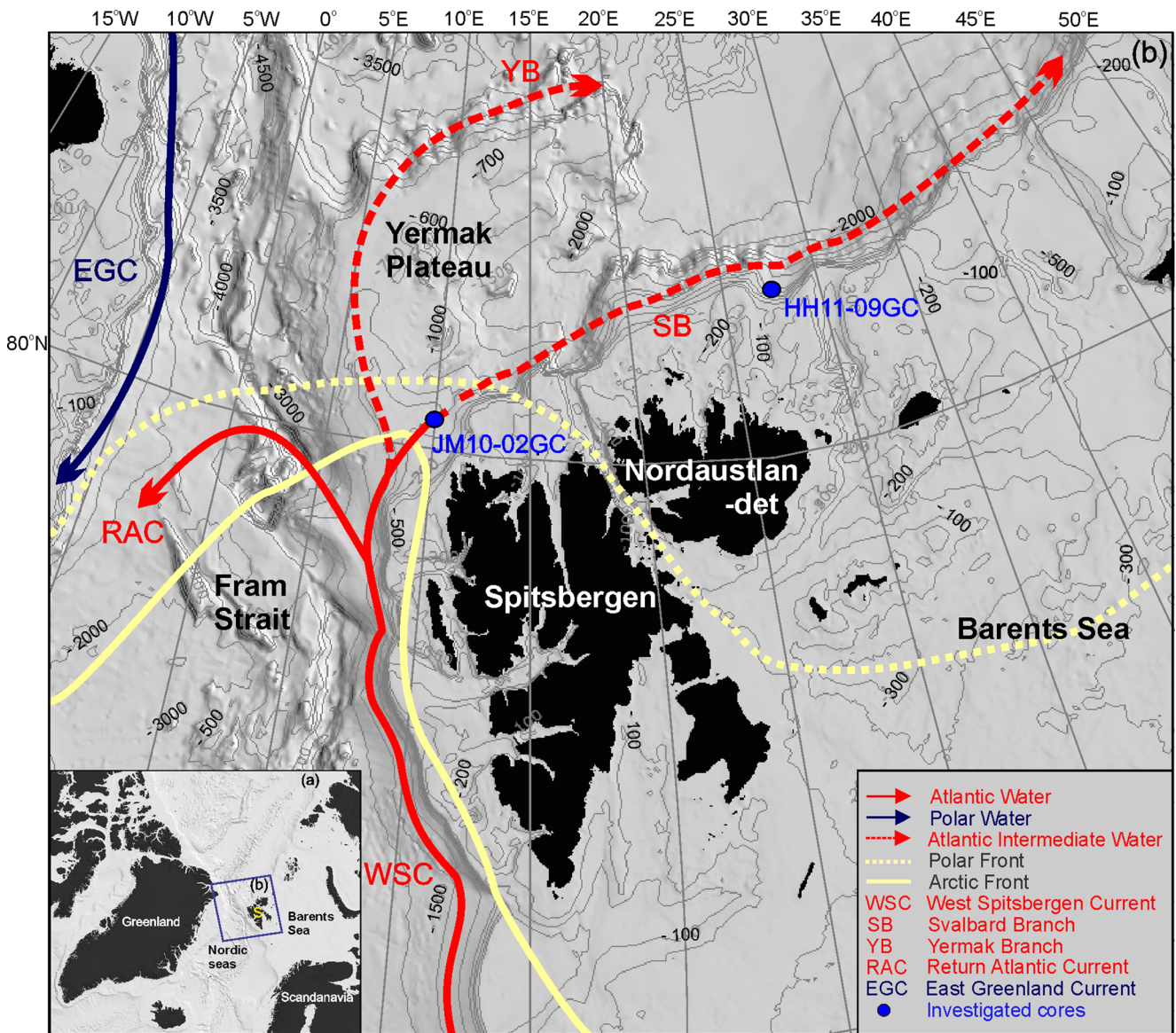
Fig. 1 **a** Location of the Svalbard archipelago (*S*) and surrounding seas. **b** Bathymetric map of the Fram Strait, northern Barents Sea margin and Yermak Plateau, with locations of cores JM10-02GC and HH11-09GC (*blue circles*) and present-day oceanography. Background bathymetry from the International Bathymetric Chart of the Arctic Ocean (IBCAO) v3 (Jakobsson et al. 2012)

have been active there since the late Miocene (Eiken and Hinz 1993). and along the western Svalbard margin since the early Pleistocene (Amundsen et al. 2011; Sarkar et al. 2011; Rebesco et al. 2013). On the north-eastern slope of the southern Yermak Plateau, at ca. 80°50′N, 9°20′E, a large moat observed at 1,200 m water depth has been suggested to represent an overflow channel produced by the northeast flowing WSC (Eiken and Hinz 1993; Vogt et al. 1994).

Materials and methods

Gravity cores JM10-02GC (80°03′N, 9°50′E, water depth 501 m, core length 3.7 m) from the southern Yermak Plateau, and

HH11-09GC (81°16′N, 26°13′E, water depth 488 m, core length 4.66 m) from the northern Svalbard continental margin north of Nordaustlandet were retrieved on cruises with R/V *Helmer Hanssen* (until 2010 known as R/V *Jan Mayen*) in September 2010 and 2011 respectively. The cores have been stored in a cool room since retrieval.

Grain size analysis

For grain size analysis, approximately 2 g of sediment were sampled at 2 cm intervals. A total of 185 samples were analysed from core JM10-02GC, and 245 samples including one sample from the core cutter and two samples from the core catcher from core HH11-09GC. From both cores, every fifth

and/or third sample was analysed twice/thrice (166 samples) to ensure reproducibility. The standard deviation estimated ranged between 0.007 and 0.6. The wet sediments were freeze-dried and treated with acetic acid and hydrogen peroxide to remove carbonate and organic matter. Fifteen samples from core HH11-09GC containing sponge spicules were treated with 1M sodium hydroxide to remove amorphous silica.

After each treatment the samples were washed with distilled water to neutralize and adjust pH to approximately 7. Before grain size analysis, 1–2 drops of Calgon (2.55 g of sodium hexametaphosphate in 25 ml of distilled water) were added to each sample, followed by treatment in an ultrasonic bath, the grains being dispersed by means of a magnetic stirrer. While the samples were stirred, approximately 5 ml of solution was pipetted out and injected into a Beckman Coulter LS 13320 Laser Particle Size Analyser. The $\overline{\text{SS}}$ was calculated geometrically on the metric scale according to the percentile statistics of Folk and Ward (1957) using the GRADISTAT software (Blott and Pye 2001).

In order to minimize the influence of sediments transported by sea ice and icebergs in the bottom current strength analysis on the slope, a statistical method proposed by Hass (2002) was used. The IRD is considered to have been derived from proximal sources and should therefore not be included in the SS analysis for bottom current conditions.

TS and TOC measurements

TS and TOC were measured on approximately 2 g sediment collected at 5 cm intervals. The wet sediment was dried overnight in an oven at 104 °C and then ground to a fine powder. Approximately 0.2–0.4 g of powdered sediment was used to determine total carbon and TS. For TOC measurement, another 0.2–0.4 g of pulverized sediment was first decalcified using 10% hydrochloric acid, washed 8 times in a porous crucible, again dried at 104 °C in an oven and then analysed in a LECO-CS200 analyser.

The content of total inorganic carbon was calculated by subtracting the TOC from the total carbon. The calcium carbonate ($CaCO_3$) content was calculated using the following equation:

$$CaCO_3(\%) = \text{total inorganic carbon}(\%) \times 8.333$$

Age model

The stratigraphic age control of cores JM10-02GC and HH11-09GC are described by Chauhan et al. (2014, 2015). The calibrated ages and tie points extracted for the age model are given in Table 1. The age model of JM10-02GC is based on AMS ^{14}C dates and correlation of the magnetic susceptibility and $\delta^{18}O$ isotope records. Nine calibrated AMS ^{14}C dates and six tie points are included in the age model. In core HH11-09G, nine calibrated AMS ^{14}C dates and five tie points are included in the age model. The AMS ^{14}C ages are measured on planktic and benthic foraminifera. The MISs boundaries are decided after Martinson et al. (1987) and Lisiecki and Raymo (2005).

Table 1 Calendar ages and additional tie points of cores JM10-02GC and HH11-09GC (after Chauhan et al. 2014, 2015). *TII* Termination II. * Basal age of core

Southern Yermak Plateau (JM10-02GC)			Upper slope north of Nordaustlandet (HH11-09GC)		
Depth (cm)	Calendar age (ka)	Comment	Depth (cm)	Calendar age (ka)	Comment
20	5.6	Radiocarbon age	31	1.5	Radiocarbon age
32	11.7	Tie point, MIS 2/1	57	3.7	Radiocarbon age
40	14.8	Radiocarbon age	72	11.7	Tie point, MIS 2/1
50	14.4	Radiocarbon age	75	11.9	Radiocarbon age
65	17.3	Radiocarbon age	165	15.3	Radiocarbon age
115	21.4	Radiocarbon age	220	16.9	Radiocarbon age
120	22.0	Radiocarbon age	240	22.0	Radiocarbon age
157	25.6	Radiocarbon age	260	22.0	Radiocarbon age
160	27.5	Radiocarbon age	280	28.0	Tie point, MIS 3/2
162	28.0	Tie point, MIS 3/2	286	29.4	Radiocarbon age
225	47.6	Radiocarbon age	335	31.8	Radiocarbon age
265	60.0	Tie point, MIS 4/3	405	60.0	Tie point, MIS 4/3
300	71.0	Tie point, MIS 5/4	465	71.0	Tie point, MIS 5/4
360	130.0	Tie point, MIS 6/5	468	74.0*	MIS 5a
368	132.0*	TII			

Additional proxies

Other proxies used for correlation are extracted from Chauhan et al. (2014, 2015). These include lithological logs, planktic oxygen and carbon isotope records, IRD distribution (>150 µm) and sedimentation rates (cm/1,000 years).

Results

Grain size distributions and SS

Southern Yermak Plateau

The grain size distributions of core JM10-02GC from the north-western Svalbard margin show that the sediments consist of ca. 40–50% clay, 30–40% silt and 10–20% sand, suggesting silt and clay as dominant components of the sediment (Fig. 2a). However, a high sand content of ca. 40% is observed at 120 cm (22 ka). Also, drop-stones (>2 mm) are observed at 300 cm (71 ka), 240 cm (52 ka) and 20–10 cm (2.8 ka). High clay contents (ca. 55%) are found at 368–360 cm (132 ka; Termination II), 255 cm (60 ka), 110 cm (20 ka) and 40 cm (14 ka; Fig. 2a).

The silt/clay ratio of core JM10-02GC ranges between 0.5 and 2 (Fig. 2a). Empirically, values lower than 1.0 represent a low ratio—for example, at 270–260 cm (MIS 4/3) and 90–80 cm (MIS 2); values of 1.0–1.5 represent an intermediate ratio, such as at 240–190 cm (MIS 3); values above 1.5 represent a high silt/clay ratio, at 20–0 cm (late Holocene). The distribution of SS shows that fine to medium silt was mainly deposited on the southern Yermak Plateau, except in the top 20 cm of the core where a high content of coarse silt is observed (Fig. 2a).

$\overline{SS}$ varies between 17.5 µm and 30 µm (Fig. 2a). Relatively coarse $\overline{SS}$ (>27 µm) is recorded at 345 cm, 335 cm and 305 cm in MIS 5, at 280 cm in MIS 4 and at 20–0 cm in the late Holocene. Relatively fine $\overline{SS}$ (<21 µm) is observed at 255 cm (60 ka) and 40 cm (14 ka).

North of Nordaustlandet

Core HH11-09GC from the northern Svalbard margin mainly consists of clayey silt and silty clay with grain size distributions more or less similar to those of core JM10-02GC. High sand contents of ca. 50% are observed between 265 and 230 cm (22 ka; Fig. 2b). A drop-stone occurs at 190 cm (15.6 ka) in the last deglaciation period. Relatively high clay contents (ca. 45%) are found at 405 cm (60 ka) and 140 cm (14 ka).

The silt/clay ratio ranges from 0.8 to 2.8 with low ratios (<1.25) observed at 405 cm (60 ka), 195 cm (15.6 ka) and 140 cm (14 ka). Relatively high ratios (>2.0) are observed at 420 cm (64 ka), 280 cm (28 ka), 260 cm (22 ka) and 130 cm (15.5 ka). The SS content shows dominance of fine and medium silt. Intervals with coarser SS content are present at 420 cm (64 ka), 280 cm (28 ka) and 260 cm (22 ka; Fig. 2b).

$\overline{SS}$ varies between 19 µm and 33 µm on the northern Svalbard margin (Fig. 2b). Relatively coarse $\overline{SS}$ (>28 µm) is recorded at 420 cm (64 ka), 280 cm (28 ka) and 260 cm (22 ka), and relatively fine $\overline{SS}$ (<20 µm) is recorded at 307.5 cm (30.5 ka), 220 cm (16.9 ka) and 200 cm (15.6 ka; Fig. 2b).

To assess the effect of IRD on the silt size fractions, the IRD-corrected $\overline{SS}$ is plotted over the original $\overline{SS}$ (µm scale) in Fig. 2a, b. The results show a weak correlation between $\overline{SS}$ and sand (weight%), with $r^2=0.17$ for core JM10-02GC and $r^2=0.37$ for core HH11-09GC. This suggests that the influence of ice rafting on sedimentation is rather weak.

Lithological facies

Based on the lithology, grain size distribution spectrum, silt/clay ratio, SS content and $\overline{SS}$, five lithological facies have been distinguished (Table 2).
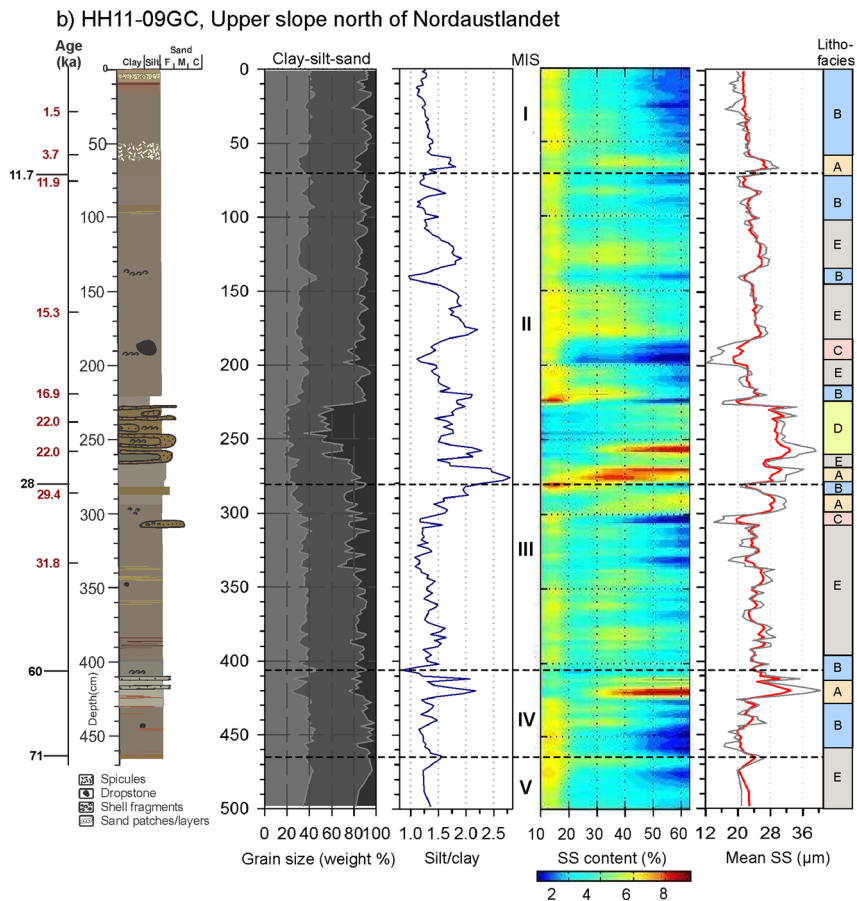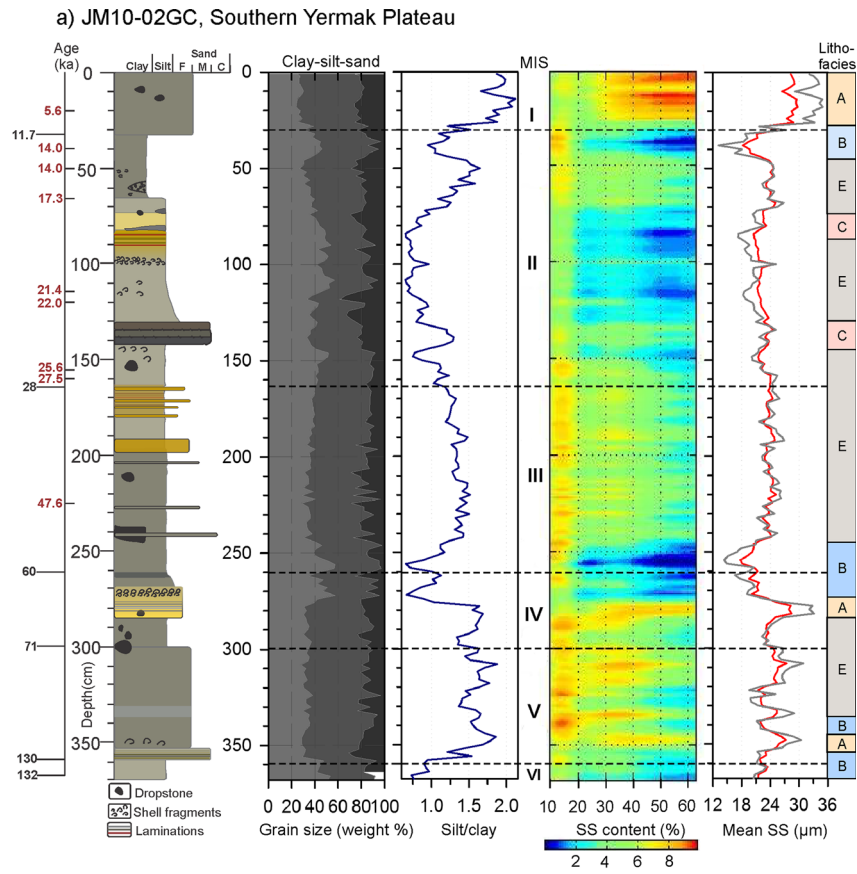
Facies A

Facies A comprises sandy silt with or without laminations. This facies has high silt/clay ratios and contains a high percentage of coarse SS. The $\overline{SS}$ size is above 28 µm. There are laminations of fine sand interbedded with mud in certain intervals (Fig. 2a, b). Facies A in core JM10-02GC contains drop-stones. The facies is interpreted to represent relatively strong bottom currents and a relatively stable and distant sediment source.

Facies B

Facies B comprises silty clay with shell fragments. This facies is characterised by low silt/clay ratios and high amounts of fine SS. The $\overline{SS}$ size is below 20 µm. The high abundance of fine silt indicates relatively weak bottom currents. Relatively high amounts of clay could be an indication of sediment input from meltwater plumes, most likely from a relatively distant source.

Facies C

Facies C comprises clayey-silty sand with or without organic material and laminations. This facies is characterised by a nearly equal amount of clay and sand together with dominance of fine SS over coarse SS. $\overline{SS}$ size varies between 24 µm and 18 µm. Elevated sand and clay contents imply sediment input from proximal sources such as melting sea ice, icebergs or nearby meltwater discharge. However, accumulation of clay from icebergs and sea ice melt-out points to a

a) JM10-02GC, Southern Yermak Plateau

b) HH11-09GC, Upper slope north of Nordaustlandet

relatively low-energy depositional environment, although sedimentation may have been facilitated by particle aggregation.

Facies D

Facies D comprises silty sand with reworked shell fragments. This facies has high silt/clay ratios with high amounts of coarse SS. The $\overline{SS}$ size is above 28 μm. The grain size distribution is mainly dominated by ca. 50% sand. These sediments are interpreted as having been deposited by down-slope gravity-driven mass movements such as those associated with turbidity currents.

Facies E

Facies E comprises clayey silt with or without drop-stones. The silt/clay ratio is moderate with wide and relatively uniform distributions of silt. The $\overline{SS}$ size is between 24 and 26 μm. Facies E is interpreted to represent contourites formed by moderate bottom current activity. Relatively low amounts of sand and clay suggest that the supply of proximal glacial sediments is minor.

TS, TOC and CaCO₃ contents

Southern Yermak Plateau

On the southern Yermak Plateau, the TS content varies between ca. 0.1 and 0.4%, except for a very high value of 1.6% between 145–135 cm (24–23 ka; Fig. 3a). The TOC content varies between 0.3% and 1.6%, with highest levels at 260 cm (ca. 60 ka; MIS 4/3 transition), 145–135 cm (24–23 ka) and 40 cm (14 ka; Fig. 3a). The CaCO₃ content varies from 1% to 12% with highest values at 150 cm (ca. 25 ka) and 80 cm (ca. 18 ka).

North of Nordaustlandet

The range of TS in core HH11-09GC is similar to that of core JM10-02GC (0.1–0.4%), with higher contents of 0.3 to 0.4% in the last deglaciation period between 210–140 cm (16–14 ka; Fig. 3b). The TOC content varies between 0.3% and 1.4% with higher values of ~1.2% at 405 cm (ca. 60 ka; MIS 4/3 transition) and 140 cm (ca. 14 ka), and 1.4% at 30–0 cm (late Holocene; Fig. 3b). Relatively high TOC contents also occur in intervals with high TS. The CaCO₃ content varies from 2%

◄ **Fig. 2** Age model (*red* AMS ^{14}C dates and *black* tie points), lithological log, clay-silt-sand contents (*light to dark grey*), silt/clay ratio, marine isotope stages (MIS), sortable silt contents (SS, 10–63 μm, in %), mean SS ($\overline{SS}$; *red and grey* uncorrected and IRD-corrected $\overline{SS}$ respectively) and lithofacies A–E in core JM10-02GC (**a**) and core HH11-09GC (**b**). Age model and lithological logs extracted from Chauhan et al. (2014, 2015)

to 16% with highest values of 11% at 415 cm (62 ka), and ~16% at 307.5 cm (30.6 ka), 280 cm (ca. 28 ka) and 224 cm (ca. 18 ka).
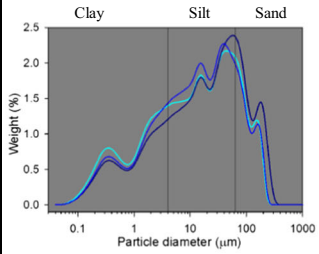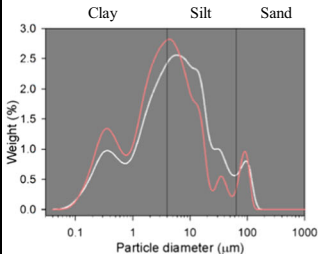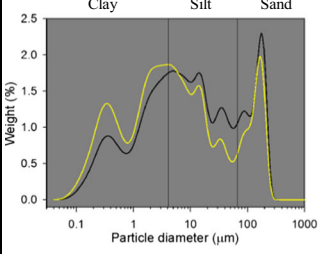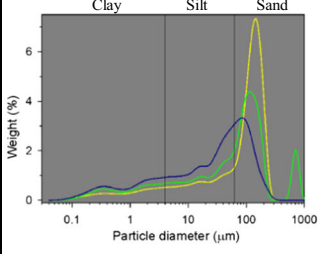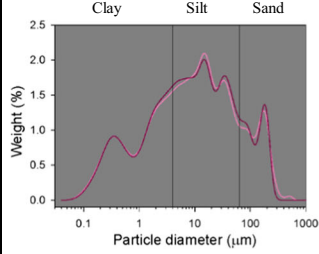
Discussion

Bottom current strength and depositional environment

In marine sediments, grain size variations can be interpreted in terms of hydraulic parameters controlling depositional processes (e.g. Flemming 1988; Kuijpers et al. 2003; Bourget et al. 2010). In addition to empirical and statistical methods, various mathematical models have been developed to analyse the composition of sediments by partitioning into several contributing components or end members (e.g. Philip and Watson 1988; Weltje 1997; Holz et al. 2004). The geological interpretation of the various components or end members in terms of their origin, supply rates and transport mechanisms, however, is rarely straightforward because sediments from different sources may have similar or partially overlapping grain size properties (Prins et al. 2002; Jonkers et al. 2015). Using merely the mean of a particular grain size for interpreting bottom currents and depositional environments is questioned by several studies (e.g. Mulder et al. 2013; Rebesco et al. 2014). Recent work by Jessen and Rasmussen (2015) shows that the use of the 'median' of SS in place of the 'mean' reduces the influence of ice rafting on the SS record considerably. In the present study, the sediment sequence has been assessed in terms of various grain size parameters (wide spectrum of grain size distribution, silt/clay ratio, content and mean of SS) in order to make inferences about the bottom current variability and depositional processes, resulting in five distinctive lithofacies. These lithofacies, together with TOC, TS, CaCO₃ and TOC/TS signatures, form the basis for palaeoenvironmental reconstruction of sedimentary environments on the northern Svalbard margin.

Intervals of sediments of facies A with a unimodal grain size distribution indicate strong bottom current activity. This facies was deposited mainly during the glacial periods of MIS 4 and MIS 2 (Table 2). Moreover, this facies was also deposited during the late Holocene (characterised as cooling period; cf. Chauhan et al. 2015) on the northern Svalbard margin. The TOC in these intervals is low and the CaCO₃ content relatively high, indicating favourable conditions for surface productivity and well ventilated bottom waters—for example, at 420 cm (62 ka) in core HH11-09GC (Fig. 2b). Sediments of facies B deposited in intervals of weak bottom current strength are recorded mainly during transition periods. The grain size distribution of facies B is unimodal with a prominent peak in the clay-sized particle range. However, it is interpreted to represent deposition of aggregated clay particles, a common phenomenon in high-latitude environments where high-salinity

Table 2 Description, grain size distribution, interpretation and examples of the five lithofacies distinguished in the two sediment cores from the north-western and northern Svalbard margin

| Litho-facies	Description	Grain size distribution	Interpretation	Examples
A	Sandy silt with or without lamination. Clay 25%, silt 50%, and sand 25%; high silt/clay ratio; high coarse silt content; coarse $\overline{SS}$		Strong bottom currents, distal sediment source, long sediment transport distance, minor influence of other, more proximal sediment sources	*Core JM10-02GC:* 26-0 cm (late Holocene) & 280–278 cm (64–63 ka) *Core HH11-09GC:* 66 cm (8 ka)
B	Silty clay or clayey silt with shell fragments. Clay 40–50%, silt 35–40% and sand 25–10%; low silt/clay ratio; very high fine silt content; fine $\overline{SS}$		Weak bottom currents, distal sediment source, long transport distance	*Core JM10-02GC:* 40 cm (14 ka) & 262–260 cm (60 ka) *Core HH11-09GC:* 100–90 cm (12.8 ka) & 140 cm (14 ka)
C	Clayey-silty sand with or without organic content and laminations. Clay 40%, silt 20% and sand 40%; relatively high silt/clay ratio; high fine silt content; medium to fine $\overline{SS}$		Relatively proximal sediment source such as nearby meltwater plume, iceberg and sea ice transported material or down-slope mass transport deposit	*Core JM10-02GC:* 92-84 cm (19 ka) & 145–130 cm (24–23 ka) *Core HH11-09GC:* 195–190 cm (15.6 ka); 220 cm (16.9 ka) & 308–307 cm (30.5 ka)
D	Silty sand with reworked shell fragments. Clay 20%, silt 25–30% and sand 50%; high silt/clay ratio; high coarse silt content; coarse $\overline{SS}$		Turbidity currents, proximal sediment sources from mass wasting processes containing reworked sediments and shell fragments	*Core HH11-09GC:* 265–240 cm (23–22 ka) Three stages during the SBIS advance – Blue - Beginning Yellow - Mid stage Green - End
E	Clayey silt with or without drop-stones. Clay 30–40%, silt 50% and sand 20–10 %; moderate silt/clay ratio; broad and relatively uniform silt content; medium $\overline{SS}$		Moderate bottom currents, long sediment transport distance, moderate influence of proximal sources	*Core JM10-02GC:* 230-170 cm (49–31 ka) *Core HH11-09GC:* 378-340 cm (48–34 ka)
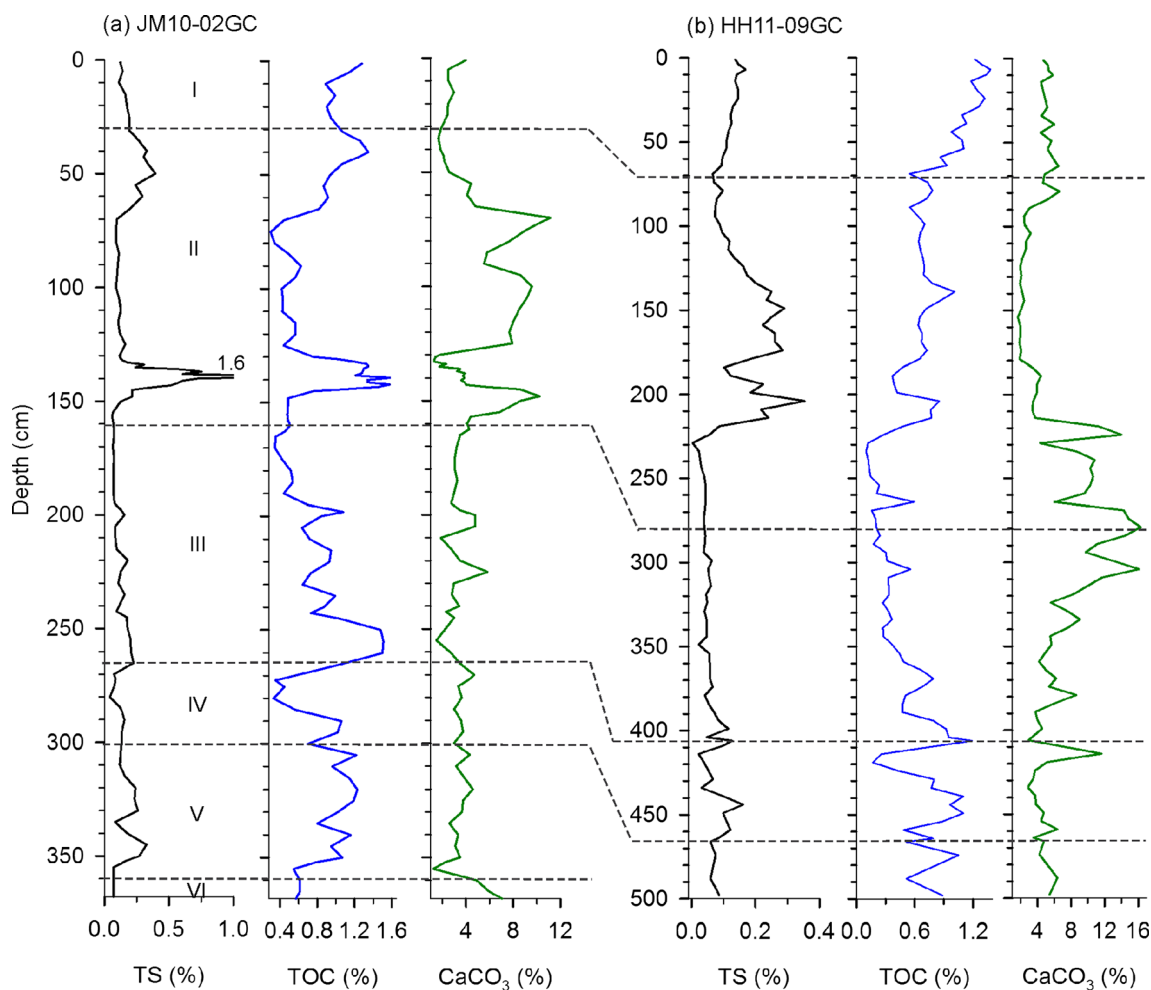
Fig. 3 Total sulphur (TS), total organic carbon (TOC) and calcium carbonate (CaCO₃) contents (%) in cores JM10-02GC (**a**) and HH11-09GC (**b**). *Grey dashed lines* Marine isotope stage (MIS) boundaries

seawater mixes with fresh glacial meltwater. The peak in fine-grained material probably results from the dispersion of aggregates in the process of sample preparation and is therefore not a reliable parameter of the local hydraulic conditions during deposition (cf. Chang et al. 2007). However, it is an informative parameter in terms of sediment source. Facies B sediments also have high contents of TOC at, for example, 260 cm in core JM10-02GC and 405 cm in core HH11-09GC (ca. 60 ka; Fig. 2a, b). Weak bottom currents can lead to oxygen deficiency at the seafloor and result in increased preservation of organic matter. Similarly, high biological productivity associated with high sedimentation rates, in particular in combination with high clay contents, binds the organic matter and preserves it from degradation (Meyers 1994; Kell et al. 1994).

Strongly mixed sediments of facies C were deposited primarily during the last glacial maximum and during the last deglaciation in MIS 2. A trimodal grain size distribution, where the peak in the clay-sized particle range often occurs together with an additional peak in the sand-sized particle range, most likely represents 'proximal' sediment sources

from sea ice or icebergs. A few intervals of facies C with high TS contents, such as at 145–135 cm (24–23 ka) in core JM10-02GC and 210–140 cm (16–14 ka) in core HH11-09GC, also show increased contents of TOC (Fig. 3a, b). Together, this suggests either that conditions were anoxic at the core site or that there was a high supply of terrigenous material rich in organic carbon and sulphur, which were preserved because of high sedimentation rates associated with the deposition of fine-grained sediments. This interpretation is supported by the low CaCO₃ contents of these intervals. Good preservation of TOC generally indicates poor ventilation, which can be unfavourable for CaCO₃ preservation. The TOC/TS ratio is another indicator of the type of depositional environment. Berner and Raiswell (1983, 1984) proposed that TOC/TS ratios of 0–5 indicate a normal marine environment and ratios of >10 indicate a freshwater environment. Consequently, ratios of 5–10 can be considered to represent a brackish environment. For example, a distinctly high ratio (36) at ca. 19 ka in core HH11-09GC implies a freshwater environment, which coincides with the beginning of the last deglaciation

(Fig. 4b). Raiswell and Berner (1985) suggested that TS measured in marine sediments mainly represents pyrite, which is usually formed in situ due to anoxic conditions, or could originate from the transport of terrigenous sediment and IRD to the core location.

Facies D is evident in core HH11-09GC between 265 cm and 240 cm (23–22 ka). The SBIS advanced onto the northern continental shelf during this period (Chauhan et al. 2015). and the three distinct peaks in the sand fraction between 265 cm and 230 cm core depths could well represent major downslope sediment transport events associated with ice sheet activity (Fig. 2b, Table 2). Facies E sediments were deposited mainly during the interglacial period of MIS 3 and MIS 5 in both cores, and partly during the glacial period of MIS 2, indicating moderate bottom current strength. In this facies, the TOC and TS contents are high in the deposits of the last deglaciation period, possibly due to high terrigenous sediment supply (Fig. 3a, b). By contrast, during MIS 3, facies E sediments display high TOC contents and low TS contents. This indicates that the source of TOC is most likely rooted in a high surface productivity, as the characteristics of facies E exclude the possibility of poor ventilation conditions. Another explanation could be that, during MIS 3, sediment supply was from different sources earmarked by lower TS contents.

Evolution during the late Quaternary

Evolution of the north-western (southern Yermak Plateau) and the northern (upper slope, north of Nordaustlandet) margins of Svalbard since MIS 5 is illustrated in Fig. 5. Results based on this study (mainly, SS and TOC) are correlated with published records of other proxies (e.g. stable isotopes and foraminiferal faunas) extracted from Chauhan et al. (2014, 2015). Variations in AW inflow and productivity are used as supportive evidence in the discussion below and also included in the schematic diagram of Fig. 5, to get a robust image of WSC flow over the upper slope near the shelf edge and the sedimentation history during the late Quaternary in close relation to the growth and decay of the SBIS.

MIS 5 (130–71 ka)

On the southern Yermak Plateau during MIS 5e (Eemian) at ca. 122 ka, high contents of IRD and high silt/clay ratios reflect increased influence of terrigenous sediment supply (Fig. 4a). The source of sediment was most likely from continuous melting of ice. In agreement with this finding, high bottom water temperature calculated by transfer functions of benthic foraminiferal species indicates the influence of warm AW (cf. Chauhan et al. 2015). During the early Weichselian from ca. 114–112 ka, TOC/TS ratios of <5 and high planktic δ^{13}C values point to high surface productivity and normal

Fig. 4 Ice-rafted debris (IRD), sedimentation rate (cm/1,000 years), silt/clay ratio, mean SS, carbon (δ^{13}C) and oxygen (δ^{18}O) isotope records of planktic foraminifers, total organic carbon (TOC) and calcium carbonate (CaCO₃) contents, TOC/CC ratio (*CC* CaCO₃) and TOC/TS ratio (*TS* total sulphur) of core JM10-02GC from the southern Yermak Plateau (**a**) and core HH11-09GC from the upper slope north of Nordaustlandet (**b**). *Grey dashed lines* Marine isotope stage (MIS) boundaries. IRD, sedimentation rates and isotopic records extracted from Chauhan et al. (2014, 2015)

marine conditions (Fig. 4a). Coarser grain size of $\overline{SS}$ implies that bottom currents were relatively strong (facies A; Table 2). These findings are in agreement with previous studies of stable isotopes, IRD and benthic foraminiferal assemblages (Wollenburg et al. 2001). which were interpreted as indicating inflow of temperate and saline AW to the northern Barents Sea margin and to the Arctic Ocean during parts of MIS 5.

During MIS 5a at ca. 78 ka, the strength of bottom currents increased on the southern Yermak Plateau (facies A, Table 2; Fig. 4a). The concomitant rise in bottom water temperature during MIS 5a has been recorded in core JM10-02GC based on foraminiferal fauna studies (Chauhan et al. 2014). Similar results of increased advection of AW were obtained in a core from the central Arctic Ocean (Spielhagen et al. 2004). At 76 ka, a peak in IRD indicates increased ice rafting and melting of icebergs, which also caused an increased supply of organic carbon (cf. high TOC content; Fig. 4a). Burial of organic matter was possibly supported by high sedimentation rates. These findings correlate well with IRD originating from an advance of the SBIS southeast of Svalbard and reaching the Yermak Plateau during late MIS 5 (Vogt et al. 2001). At ca. 74 ka on the northern Svalbard margin, the presence of facies B sediments and low planktic δ^{18}O values indicate reduced bottom current strength and influence of freshwater at the surface (Fig. 4b, Table 2). Micropalaeontological studies of core HH11-09GC show that warm AW advected during this period, which may have accelerated the melting process and supply of fresh water, causing a weakening of bottom current strength (Chauhan et al. 2015).

MIS 4 (71–60 ka)

On the southern Yermak Plateau, early MIS 4 is characterised by deposits of facies E sediment, implying moderate bottom current strength (Table 2). The presence of drop-stones and peaks in IRD indicate the influence of ice rafting, which also apparently affected the surface productivity (low planktic δ^{13}C values; Figs. 2a, 4a). By contrast, on the upper continental slope north of Nordaustlandet, sediments of facies B indicate weak bottom current strength, whereas high planktic δ^{13}C values point to high surface productivity (Table 2, Fig. 4b). In agreement with this finding, Chauhan et al. (2014, 2015) suggested that the inflow of subsurface AW was low at the southern Yermak Plateau, and even further reduced at the northern

(a) JM10-02GC - Southern Yermak Plateau
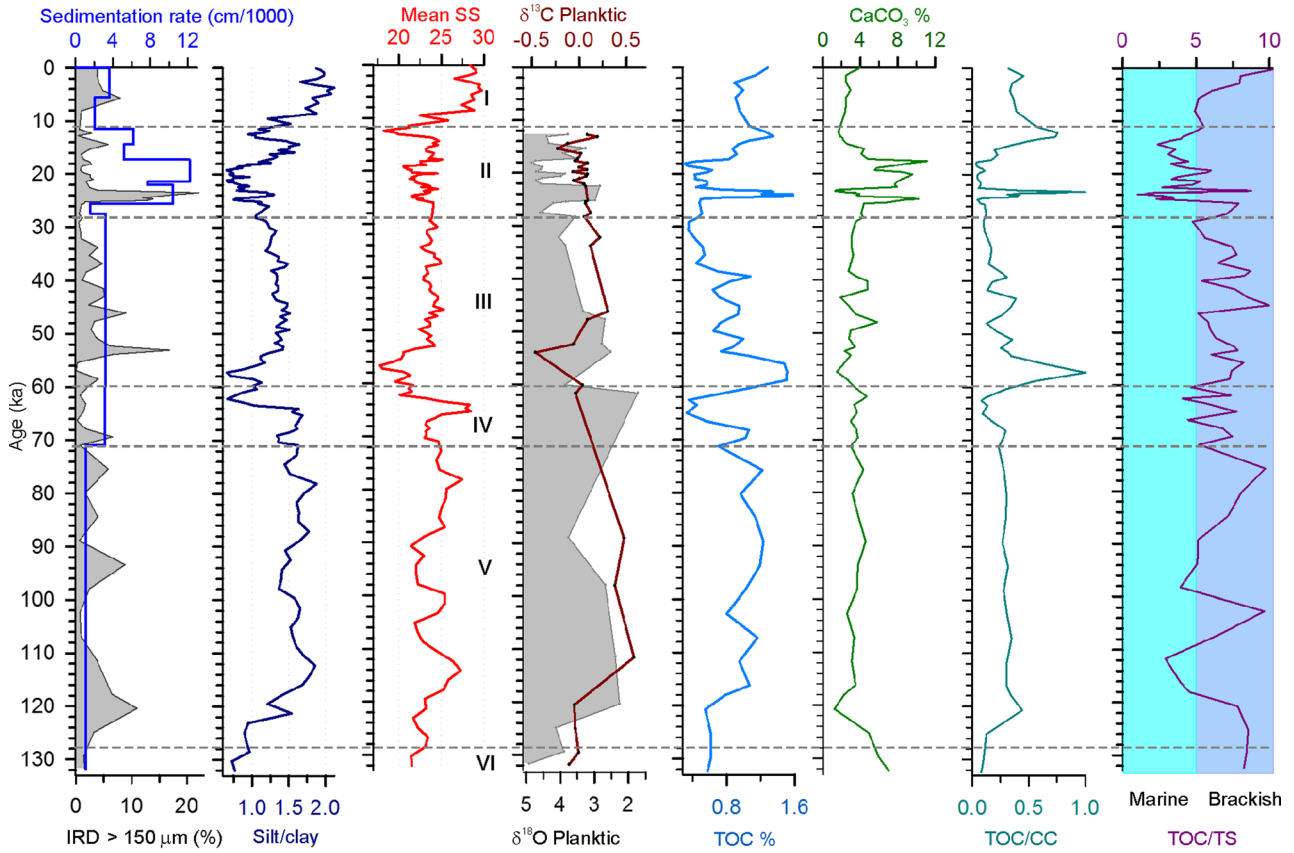
(b) HH11-09GC - Upper slope north of Nordaustlandet
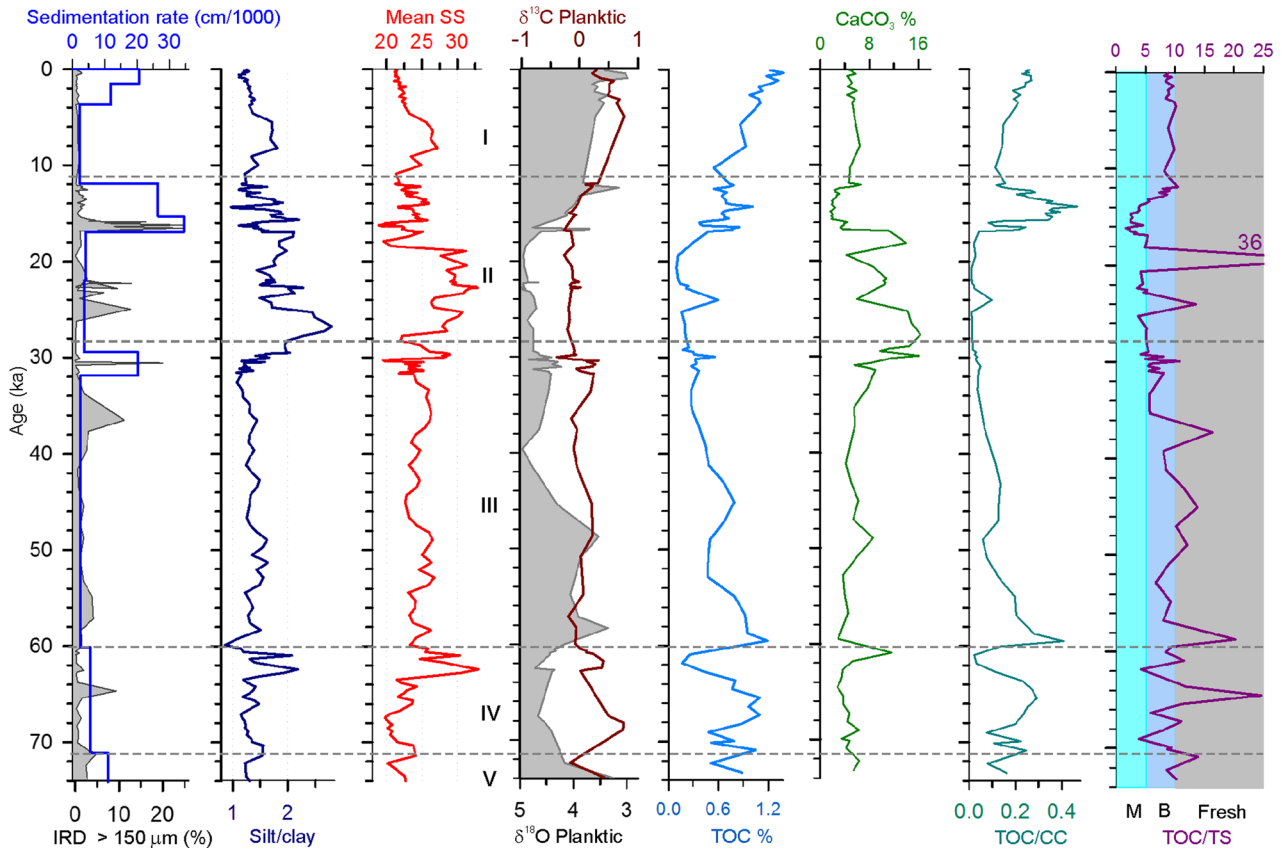
Svalbard margin. Records from the Nordic Seas indicate stronger influence of warm AW south of Svalbard supplying moisture for ice sheet growth (Hebbeln and Wefer 1997; Hebbeln et al. 1998). As a result, the SBIS advanced towards the shelf edge north of Nordaustlandet at ca. 65 ka, which is marked by an IRD peak, a high TOC content and a TOC/TS ratio >10 in the present study (Fig. 4b). A high TOC/CC ratio indicates decrease in $CaCO_3$ preservation due to the SBIS advance.

On the north-western and northern Svalbard margins, an abrupt increase in $\overline{SS}$ (facies A) occurs in two short time intervals at ca. 64 ka and 62 ka respectively (Fig. 4a, b, Table 2). These events are interpreted to represent strong bottom currents, which can be linked to (1) the formation of dense water due to super-cooling underneath large floating ice shelves, (2) excess heat loss in open water conditions or (3) brine rejection during sea ice formation (cf. Rodehacke et al. 2007). Another explanation for relatively coarse $\overline{SS}$ could be meltwater discharge beneath an ice shelf (facies C). In the modern oceanographic setting, shelf dense waters form during the winter season due to excess heat loss under open water conditions at the southern Yermak Plateau (Frank Nilsen, UNIS, pers. comm.). It is suggested that dense water formation best explains the sediments of facies A (Table 2). The core interval centred at ca. 64 ka is barren of benthic foraminifera northwest of Svalbard (Chauhan et al. 2014). Along the northern Svalbard margin, coarser $\overline{SS}$ and facies A are associated with high $CaCO_3$ contents and relatively high planktic $\delta^{13}C$ values (Fig. 4b). High surface productivity could be due to open water conditions or upwelling of nutrient-rich bottom water, which can also cause re-deposition of sand. Based on foraminiferal fauna and isotope studies, Chauhan et al. (2015) found indications that a polynya was formed around 62 ka. The strong bottom current activity and deposition of sand layers could have been associated with brine rejection during extensive sea ice formation following the period of high surface productivity during polynya formation.

The MIS 4/3 transition at 60 ka is characterised by facies B and a pronounced increase in TOC contents at both core locations (Fig. 4a, b, Table 2). Together with a very low silt/clay ratio, these parameters indicate reduced bottom current strength and weaker ocean circulation, which enabled excess clay to settle from suspension. The fine sediment texture and apparently sub-oxic conditions may have facilitated preservation of organic carbon. Low $\delta^{18}O$ values, a markedly high TOC/CC ratio, a TOC/TS ratio >10 (Fig. 4a, b) and similar results of other studies (cf. Rasmussen et al. 2014a) support a strong influence of meltwater at the surface, which may have reduced vertical water exchange and prevented oxygen-enriched water reaching the bottom layers at both the north-western and northern Svalbard margins. The interval correlates with Heinrich event H6 (Chauhan et al. 2015).

Fig. 5 a–l Sketch illustrating the interplay of climatic, oceanographic and ice sheet processes, and their effects on the sedimentary environment of the north-western (southern Yermak Plateau) and northern (north of Nordaustlandet) Svalbard margins at various key time periods since MIS 5. Atlantic Water inflow and productivity data are extracted from Chauhan et al. (2014, 2015). *SBIS* Svalbard-Barents Sea ice sheet ▶

MIS 3 (60–28 ka)

Facies E dominate in both cores during MIS 3 (Table 2). At the southern Yermak Plateau, the stable current regime indicated by facies E began at ca. 54 ka, after the deposition of IRD from the retreating SBIS diminished (Fig. 4a). Evidence for retreat of the SBIS during early MIS 3 has also been recorded in the Fram Strait, the western Svalbard margin, the northern Barents Sea margin and the central Arctic Ocean between 60 ka and 52 ka (Lloyd et al. 1996; Nørgaard-Pedersen 1997; Hebbeln and Wefer 1997; Darby et al. 1997; Knies et al. 2001). Chauhan et al. (2014) suggested that the southern Yermak Plateau was influenced by seasonal sea ice cover throughout MIS 3. Studies show that surface productivity is generally higher at the sea ice margin and in areas of seasonal sea ice cover (Carstens et al. 1997; Pados and Spielhagen 2014). Increased productivity, in turn, boosts the supply of organic carbon to the sea bottom and can result in dissolution of $CaCO_3$ (Archer et al. 1989). The high TOC content in both cores is thus interpreted to reflect periods of marginal ice conditions (Fig. 4a, b). These intervals also correlate with foraminifer-barren intervals within MIS 3, indicating dissolution (Chauhan et al. 2014, 2015).

Along the northern Svalbard margin at ca. 37 ka, a TOC/TS ratio >10 indicates the presence of a freshwater environment. Together with an IRD peak at ca. 35 ka, the evidence points to decay of the SBIS (Fig. 4b). The disintegration of the SBIS can be associated with an influx of warm AW during this period, as shown by foraminiferal faunas (Chauhan et al. 2015). Somewhat later at 31–30 ka, an abrupt drop in $\overline{SS}$ from medium to fine SS points to a grounding event (Fig. 4b; see below).

Late MIS 3 grounding event

In core HH11-09GC from the upper continental slope north of Nordaustlandet at ca. 30.5 ka (307–308 cm core depth), a prominent IRD peak, high sedimentation rates and an abrupt decrease in $\overline{SS}$ were recorded (Figs. 2b, 4b). Initially, $\overline{SS}$ decreased abruptly from 25 μm to 19 μm for a short interval, followed by a distinct increase in $\overline{SS}$ to 25–28 μm. This interval belongs to facies C (Table 2). Deposition of a medium-sized sand lens suggests that the sand was probably derived from a proximal source and thus could have been deposited by down-slope mass transport rather than by strong lateral bottom
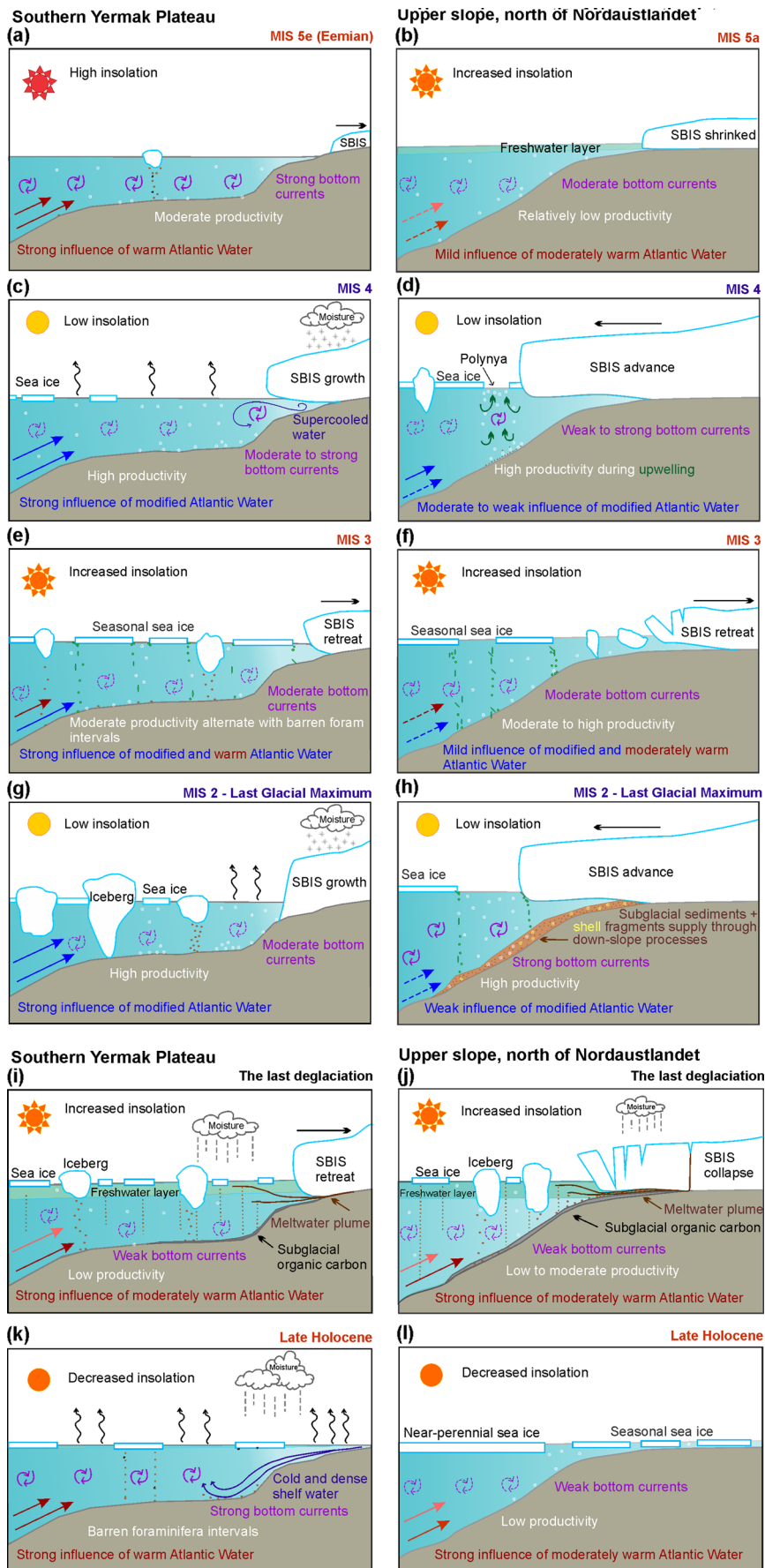
currents. The older radiocarbon date (35.6 ka) obtained from the sand layer (Chauhan et al. 2015) supports this interpretation.

The down-slope sediment mass-transport event could have been caused by an advance of the SBIS or local sediment failures at the shelf edge. The relative sea-level record by Arz et al. (2007) shows that, from ca. 32 ka to ca. 30.6 ka, the sea level gradually dropped and lasted for only a short period (~500 years; Fig. 6). In core HH11-09GC, the
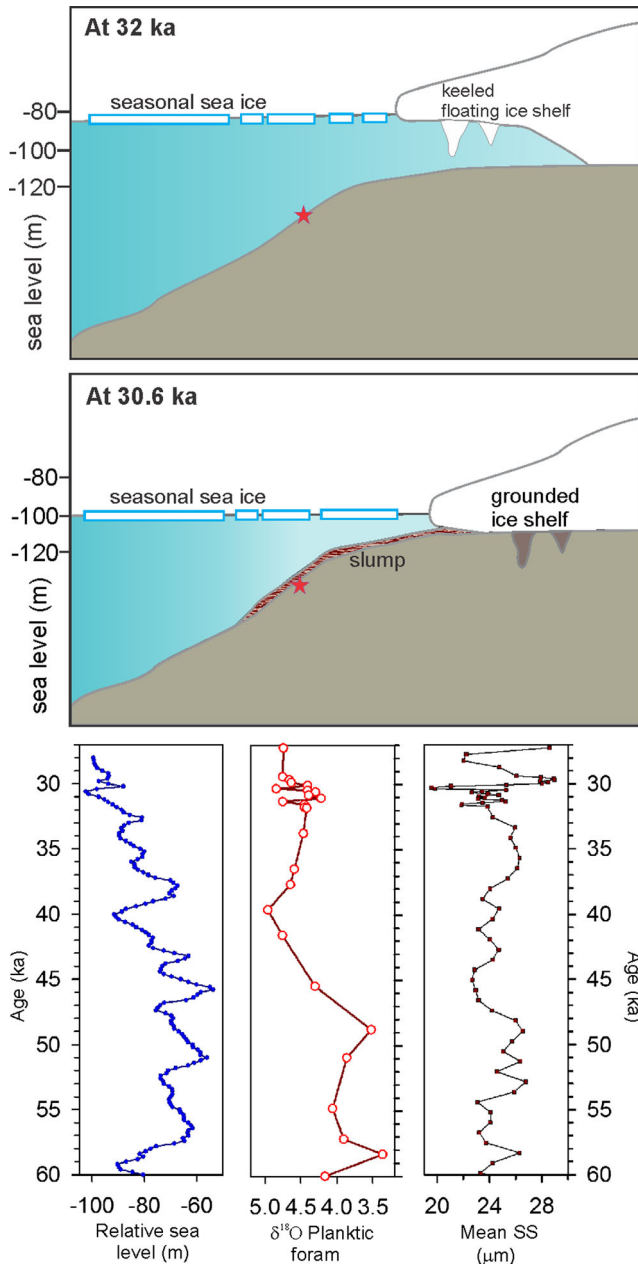

Fig. 6 Schematic diagram (not to scale) showing conditions during late MIS 3 at the core site HH11-09GC (*red star*) on the upper slope north of Nordaustlandet. *Blue curve* Relative sea level (m) extracted from Arz et al. (2007). *red curve* oxygen isotope record of this core during MIS 3 (60–28 ka) extracted from Chauhan et al. (2015). *dark red curve* SS mean record of MIS 3 (this study). For details, refer to the Discussion section

fluctuation in planktic δ^{18}O values between ca. 30.5–30 ka supports the sea-level record (Fig. 6). Glacial landforms near the continental shelf edge in the vicinity of the core site feature ca. 12 km long, 20–35 m deep and 0.5–1 km wide grooves (Noormets et al. 2012). The compact sediments recovered from the grooves have a basal age of 30 ka (unpublished data), which closely corresponds to the brief period of low sea-level stand. This suggests that the falling sea level at ca. 30.6 ka could have resulted in sediment mass failures on the upper slope, possibly associated with ice sheet margin processes (Fig. 6). Thin sand layers in core JM10-02GC from the southern Yermak Plateau suggest that a similar event could have occurred on the north-western Svalbard margin at approximately the same time (Fig. 2a).

MIS 2 (28–11.7 ka)

Sediments of facies E were deposited at the beginning of MIS 2 on the southern Yermak Plateau (Table 2). Surface productivity increased between 24 ka and 20 ka (cf. high CaCO$_3$ content; Fig. 4a). This period correlates well with the timing of AW advection and high productivity zones in the Nordic Seas, the western Svalbard margin and the southern Yermak Plateau (Hebbeln et al. 1994; Elverhøi et al. 1995; Dokken and Hald 1996; Hebbeln and Wefer 1997; Hald et al. 2001; Chauhan et al. 2014). From 24–23 ka the TOC content increased abruptly, correlating to a banded IRD layer (Figs. 2a, 4a). The IRD originated from the southern Svalbard region and from mass-wasting events along the western Svalbard margin due to the advance of the SBIS (Andersen et al. 1996). The event has been traced all along the western Svalbard margin in the form of an IRD band with decreasing thickness (Vogt et al. 2001; Jessen et al. 2010; Chauhan et al. 2014). Moreover, sediment of the IRD layer is characterised by facies C, suggesting that the sediment source was proximal (Table 2).

Along the northern Svalbard margin, the environmental conditions were slightly different. Here, sediments of facies A and high silt/clay ratios between 28 ka and 24 ka indicate relatively strong bottom currents (Fig. 4b, Table 2). The increase in CaCO$_3$ content points to good ventilation (Fig. 4b). Knies and Stein (1998) documented a high productivity during this period in a core from the lower slope of the northern Svalbard margin. The TOC content also increased at the northern Svalbard margin, correlating in time with the deposition of the TOC-rich IRD layer at ca. 24 ka on the southern Yermak Plateau. The high TOC indicates decreased bottom ventilation probably due to reduction in bottom current strength (decrease in $\overline{SS}$; Fig. 4b). The period correlates with Heinrich event H2, where a meltwater layer at the surface led to a stratified water column (Chauhan et al. 2015).

Above this interval at around 22 ka, sediments of facies D with high sand and high CaCO₃ contents indicate deposition from down-slope transported sediments associated with a relatively strong bottom current regime (Figs. 2b, 4b, Table 2). The grain size distribution during this event resembles the sediments described by Anderson et al. (1980) as "moderately to poorly sorted 'residual marine sediment' consisting of abundant marine fossils and where the fine component of silt has been winnowed due to strong bottom currents". Facies D as well as foraminiferal and isotope studies suggest that the SBIS advanced during 23–22 ka and caused re-deposition of continental shelf sediments containing shell fragments on the upper slope (Chauhan et al. 2015).

Last deglaciation (19–11.7 ka)

At the southern Yermak Plateau, the minimum silt/clay ratio at ca. 19 ka indicates high input of clay either due to reduced bottom current strength or from meltwater discharge (Fig. 4a). However, facies C sediments and high sedimentation rates during this period indicate that the sediment supply was from a relatively proximal source (Fig. 4a, Table 2). Despite the favourable conditions, TOC content was low, probably due to high turbidity (Fig. 4a). Similarly, on the northern Svalbard margin the $\overline{SS}$ dropped abruptly from 30 μm to 22 μm, and the TOC/TS ratios increased to around 36 at ca. 19 ka, indicating a major decline in bottom current strength and a freshwater environment, probably due to a strong outburst of meltwater (Fig. 4b). This period is interpreted to represent the beginning of the last deglaciation. High turbidity due to meltwater discharge could explain the absence of foraminifera at the southern Yermak Plateau (Chauhan et al. 2014) and the decline in the overall flux of foraminifers in the upper slope sediments north of Nordaustlandet (Chauhan et al. 2015).

From 17.3 ka (north-western Svalbard margin) and 16.9 ka (northern Svalbard margin) onwards, sedimentation of terrigenous sediments increased (high silt/clay ratio) in association with high TOC and TS contents. The source of sediments and TOC was probably from melting sea ice/icebergs (low δ¹⁸O values; Fig. 4a, b). These periods also coincide with the interval equivalent to Heinrich event 1 (Chauhan et al. 2014, 2015). At 15.6 ka on the northern Svalbard margin, facies C sediments with a prominent IRD peak and a high sedimentation rate mark the period of major disintegration of the SBIS and the onset of the Bølling-Allerød interstadial (Table 2, Fig. 4b). This is in agreement with findings from foraminiferal studies (Chauhan et al. 2015). Similarly, in a sediment core from the lower slope along the northern Svalbard margin, a gradual increase in TOC content was recorded between 15.6 ka and 11.2 ka (Knies and Stein 1998). Sedimentological studies from other regions also show that the strength of the outer shelf Iberian Poleward Current

(Bender et al. 2012) and the Labrador Current (Marshall et al. 2014) increased at ca. 15.5 ka, in turn influencing the Atlantic Meridional Overturning Circulation. At 14–13 ka, bottom current strength was significantly reduced at both core locations (facies B and high TOC/CC ratios) probably due to meltwater discharge (Fig. 4a, b). This event was recorded in several marine records around Svalbard (Birgel and Hass 2004; Jessen et al. 2010; Rüther et al. 2012; Hormes et al. 2013; Kristensen et al. 2013; Lucchi et al. 2013). The released meltwater raised the sea level and, according to Weaver et al. (2003). this would have strengthened the oceanic circulation and accelerated the climatic warming during the Bølling-Allerød interstadial.

Holocene

The Holocene section of both cores consists of late Holocene sediments, whereas early Holocene sediments are absent (Fig. 2a, b). This is probably due to strong bottom currents, which either prevented the accumulation of sediments at that time or, alternatively, eroded sediments deposited earlier. Recent studies from the western Barents Sea margin indicate an influence of strong bottom currents during the Holocene, as inferred from calcareous sands and shell debris (Rüther et al. 2012). Lau (1994) suggested that sediment deposition also depended on water temperature, where lower temperatures result in lower particle settling velocities and vice versa (cf. also Krögel and Flemming 1998). Several studies have characterised the early Holocene as a warm period associated with stronger advection of relatively warm AW to the Nordic Seas and to the Hinlopen Strait (Polyak and Mikhailov 1996; Slubowska et al. 2005; Aagaard-Sørensen et al. 2014; Rasmussen et al. 2014b), whereas the late Holocene has been considered as a relatively cold period with a bottom environment less influenced by AW (Slubowska et al. 2005; Kristensen et al. 2013).

In this study, different oceanographic regimes and surface conditions were recorded at both core locations during the late Holocene (Fig. 4a, b). On the southern Yermak Plateau, facies A sediments, high silt/clay ratios and low TOC contents indicate more vigorous bottom currents (Fig. 4a, Table 2). The reason for stronger currents could have been excessive heat loss from the AW to the atmosphere, which resulted in the formation of cold and dense water cascading down-slope and causing strong bottom currents and high turbidity at the bottom. Simultaneously, on the upper slope north of Nordaustlandet, facies E sediments and relatively low silt/clay ratios point to moderate to weak current activity, probably due to further reduced influence of AW and an expansion of sea ice cover (Fig. 4b, Table 2). Foraminiferal faunas also indicate near-perennial to

seasonal sea ice cover (Chauhan et al. 2015). The differences in the depositional environments at the two core locations are interpreted as resulting from different influences of southward flowing Polar Water and northward flowing AW.

Conclusions

1. Oceanographic conditions and ice sheet processes have exerted first-order control on sediment properties in the contourite-dominated depositional environment on the northern Svalbard margin during the late Quaternary.

2. Five lithofacies characteristic of different contouritic depositional environments were distinguished in two sediment cores. These lithofacies, based on grain size distribution spectra, silt/clay ratio, content and mean of SS, can be useful in reconstructing past bottom current activity from similar settings worldwide. This aspect awaits confirmation in future research.

3. Coarsening of mean SS and strong bottom current activity primarily occurred due to dense water formation and are pronounced during intervals of glacial periods and the late Holocene. Fining of mean SS with higher organic carbon preservation and low $CaCO_3$ content reflect limited water exchange and reduced bottom current strength during transitional periods, such as at MIS 4/3 (60 ka) and MIS 2/1 (14 ka). The MIS 3 interglacial period and intervals in MIS 5 are mainly characterised by medium to fine silt and moderate bottom current strength with presence of dropstones. Ice rafting is more evident during the last glacial maximum than in MIS 4.

4. Based on grain size distribution, mean SS and other supportive parameters (planktic $\delta^{18}O$ values, relative sea-level record and glacial landforms), evidence of a grounding event during late MIS 3 on the northern Svalbard margin is documented for the first time.

5. Due to the physiographic setting, sedimentation rate was higher on the northern Svalbard margin than on the southern Yermak Plateau during the last deglaciation.

6. In addition to sediment input from sea ice and icebergs, sedimentation on the southern Yermak Plateau was mostly influenced by contour currents, whereas on the upper slope north of Nordaustlandet the interaction of contour currents and down-slope mass-flow processes dominated the environment.

Compliance with ethical standards

Conflict of interest The authors declare that there is no conflict of interest with third parties.

References

Aagaard-Sørensen S, Husum K, Hald M, Marchitto T, Godtliebsen F (2014) Sub sea surface temperatures in the Polar North Atlantic during the Holocene: planktic foraminiferal Mg/Ca temperature reconstructions. The Holocene 24:93–103. doi:10.1177/0959683613515730

Amundsen IMH, Blinova M, Hjelstuen BO, Mjelde R, Haflidason H (2011) The Cenozoic western Svalbard margin: sediment geometry and sedimentary processes in an area of ultraslow oceanic spreading. Mar Geophys Res 32:441–453. doi:10.1007/s11001-011-9127-z

Andersen ES, Dokken TM, Elverhøi A, Solheim A, Fossen I (1996) Late Quaternary sedimentation and glacial history of the western Svalbard continental margin. Mar Geol 133:123–156. doi:10.1016/0025-3227(96)00022-9

Anderson J, Kurtz D, Domack E, Balshaw K (1980) Glacial and glacial marine sediments of the Antarctic continental shelf. J Geol 88:399–414. doi:10.1130/0091-7613(1995)023<0580:GMADSO>2.3.CO;2

Archer D, Emerson S, Reimers C (1989) Dissolution of calcite in deep-sea sediments: pH and O^2 microelectrode results. Geochim Cosmochim Acta 53:2831–2845. doi:10.1016/0016-7037(89)90161-0

Arz HW, Lamy F, Ganopolski A, Nowaczyk N, Pätzold J (2007) Dominant Northern Hemisphere climate control over millennial-scale glacial sea-level variability. Quat Sci Rev 26:312–321. doi:10.1016/j.quascirev.2006.07.016

Bender V, Hanebuth T, Mena A, Baumann K-H, Francés G, Dobeneck T (2012) Control of sediment supply, palaeoceanography and morphology on late Quaternary sediment dynamics at the Galician continental slope. Geo-Mar Lett 32:313–335. doi:10.1007/s00367-012-0282-2

Berner RA, Raiswell R (1983) Burial of organic carbon and pyrite sulfur in sediments over Phanerozoic time: a new theory. Geochim Cosmochim Acta 47:855–862. doi:10.1016/0016-7037(83)90151-5

Berner RA, Raiswell R (1984) C/S method for distinguishing freshwater from marine sedimentary rocks. Geology 12:365–368

Birgel D, Hass HC (2004) Oceanic and atmospheric variations during the last deglaciation in the Fram Strait (Arctic Ocean): a coupled high-resolution organic-geochemical and sedimentological study. Quat Sci Rev 23:29–47. doi:10.1016/j.quascirev.2003.10.001

Blott SJ, Pye K (2001) GRADISTAT: a grain size distribution and statistics package for the analysis of unconsolidated sediments. Earth Surf Process Landf 26:1237–1248. doi:10.1002/esp.261

Bourget J, Zaragosi S, Ellouz-Zimmermann S, Ducassou E, Prins MA, Garlan T, Launfumey V, Schneider LJ, Rouillard P, Giraudeau J (2010) Highstand vs. lowstand turbidite system growth in the Makran active margin: imprints of high-frequency external controls on sediment delivery mechanisms to deep water systems. Mar Geol 274:187–208. doi:10.1016/j.margeo.2010.04.005

Canfield DE (1994) Factors influencing organic carbon preservation in marine sediments. Chem Geol 114:315–329. doi:10.1016/0009-2541(94)90061-2

Canfield DE, Jørgensen BB, Fossing H, Glud R, Gundersen J, Ramsing NB, Thamdrup B, Hansen JW, Nielsen LP, Hall POJ (1993) Pathways of organic carbon oxidation in three continental margin sediments. Mar Geol 113:27–40. doi:10.1016/0025-3227(93)90147-N

Carstens J, Hebbeln D, Wefer G (1997) Distribution of planktic foraminifera at the ice margin in the Arctic (Fram Strait). Mar Micropaleontol 29:257–269. doi:10.1016/S0377-8398(96)00014-X

Chang TS, Flemming BW, Bartholomä A (2007) Distinction between sortable silts and aggregated particles in muddy intertidal sediments of the East Frisian Wadden Sea, southern North Sea. Sediment Geol 202:453–463. doi:10.1016/j.sedgeo.2007.03.009

Chauhan T, Rasmussen TL, Noormets R, Jakobsson M, Hogan KA (2014) Glacial history and paleoceanography of the southern Yermak Plateau since 132 ka BP. Quat Sci Rev 92:155–169. doi:10.1016/j.quascirev.2013.10.023

Chauhan T, Rasmussen TL, Noormets R (2015) Palaeoceanography of the Barents Sea continental margin, north of Nordaustlandet, Svalbard, during the last 74 ka. Boreas. doi:10.1111/bor.12135

Darby DA, Bischof JF, Jones GA (1997) Radiocarbon chronology of depositional regimes in the western Arctic Ocean. Deep-Sea Res II Top Stud Oceanogr 44:1745–1757. doi:10.1016/S0967-0645(97)00039-8

Dokken TM, Hald M (1996) Rapid climatic shifts during isotope stages 2–4 in the Polar North Atlantic. Geology 24:599–602. doi:10.1130/0091-7613(1996)024<0599:RCSDIS>2.3.CO;2

Dowdeswell JA, Evans J, Ó Cofaigh C (2010) Submarine landforms and shallow acoustic stratigraphy of a 400 km-long fjord-shelf-slope transect, Kangerlussuaq margin, East Greenland. Quat Sci Rev 29:3359–3369. doi:10.1016/j.quascirev.2010.06.006

Eiken O, Hinz K (1993) Contourites in the Fram Strait. Sediment Geol 82:15–32. doi:10.1016/0037-0738(93)90110-Q

Elverhøi A, Andersen ES, Dokken T, Hebbeln D, Spielhagen R, Svendsen JI, Sørflaten M, Rørnes A, Hald M, Forsberg CF (1995) The growth and decay of the Late Weichselian Ice Sheet in Western Svalbard and adjacent areas based on provenance studies of marine sediments. Quat Res 44:303–316. doi:10.1006/qres.1995.1076

Emerson S, Hedges JI (1988) Processes controlling the organic carbon content of open ocean sediments. Paleoceanography 3:621–634. doi:10.1029/PA003i005p00621

Fahrbach E, Meincke J, Østerhus S, Rohardt G, Schauer U, Tverberg V, Verduin J (2001) Direct measurements of volume transports through Fram Strait. Polar Res 20:217–224. doi:10.1111/j.1751-8369.2001.tb00059.x

Flemming BW (1988) Process and pattern of sediment mixing in a microtidal coastal lagoon along the west coast of South Africa. In: de Boer PL, van Gelder A, Nio SD (eds) Tide-influenced sedimentary environments and facies. D Reidel, Dordrecht, pp 275–288

Folk RL, Ward WC (1957) Brazos River bar: a study in the significance of grain size parameters. J Sediment Res 27:3–26. doi:10.1306/74D70646-2B21-11D7-8648000102C1865D

Gröger M, Henrich R, Bickert T (2003) Glacial–interglacial variability in lower North Atlantic deep water: inference from silt grain-size analysis and carbonate preservation in the western equatorial Atlantic. Mar Geol 201:321–332. doi:10.1016/S0025-3227(03)00263-9

Hald M, Dokken T, Mikalsen G (2001) Abrupt climatic change during the last interglacial–glacial cycle in the polar North Atlantic. Mar Geol 176:121–137. doi:10.1016/S0025-3227(01)00158-X

Hass HC (2002) A method to reduce the influence of ice-rafted debris on a grain size record from northern Fram Strait, Arctic Ocean. Polar Res 21:299–306. doi:10.1111/j.1751-8369.2002.tb00084.x

Hebbeln D, Wefer G (1997) Late Quaternary paleoceanography in the Fram Strait. Paleoceanography 12:65–78. doi:10.1029/96PA02753

Hebbeln D, Dokken T, Andersen ES, Hald M, Elverhøi A (1994) Moisture supply for northern ice-sheet growth during the Last Glacial Maximum. Nature 370:357–360. doi:10.1038/370357a0

Hebbeln D, Henrich R, Baumann KH (1998) Paleoceanography of the last interglacial/glacial cycle in the Polar North Atlantic. Quat Sci Rev 17:125–153. doi:10.1016/S0277-3791(97)00067-X

Hedges JI, Keil RG (1995) Sedimentary organic matter preservation: an assessment and speculative synthesis. Mar Chem 49:81–115. doi:10.1016/0304-4203(95)00008-F

Holz C, Stuut JW, Henrich R (2004) Terrigenous sedimentation processes along the continental margin off NW Africa: implications from grain-size analysis of seabed sediments. Sedimentology 51:1145–1154. doi:10.1111/j.1365-3091.2004.00665.x

Hormes A, Gjermundsen EF, Rasmussen TL (2013) From mountain top to the deep sea—deglaciation in 4D of the northwestern Barents Sea ice sheet. Quat Sci Rev 75:78–99. doi:10.1016/j.quascirev.2013.04.009

Howe JA, Shimmield TM, Harland R (2008) Late Quaternary contourites and glaciomarine sedimentation in the Fram Strait. Sedimentology 55:179–200. doi:10.1111/j.1365-3091.2007.00897.x

Jakobsson M, Mayer L, Coakley B, Dowdeswell JA, Forbes S, Fridman B, Hodnesdal H, Noormets R, Pedersen R, Rebesco M, Schenke HW, Zarayskaya Y, Accettella D, Armstrong A, Anderson RM, Bienhoff P, Camerlenghi A, Church I, Edwards M, Gardner JV, Hall JK, Hell B, Hestvik O, Kristoffersen Y, Marcussen C, Mohammad R, Mosher D, Nghiem SV, Pedrosa MT, Travaglini PG, Weatherall P (2012) The International Bathymetric Chart of the Arctic Ocean (IBCAO) Version 3.0. Geophys Res Lett 39: L12609. doi:10.1029/2012GL052219

Jessen SP, Rasmussen TL (2015) Sortable silt cycles in Svalbard slope sediments 74–0 ka. J Quat Sci. doi:10.1002/jqs.2807

Jessen SP, Rasmussen TL, Nielsen T, Solheim A (2010) A new Late Weichselian and Holocene marine chronology for the western Svalbard slope 30,000–0 cal years BP. Quat Sci Rev 29:1301–1312. doi:10.1016/j.quascirev.2010.02.020

Jonkers L, Barker S, Hall IR, Prins MA (2015) Correcting for the influence of ice-rafted detritus on grain size-based paleocurrent speed estimates. Paleoceanography 30:1347–1357. doi:10.1002/2015PA002830

Kell RG, Montluçon DB, Prahl FG, Hedges JI (1994) Sorptive preservation of labile organic matter in marine sediments. Nature 370:549–552. doi:10.1038/370549a0

Knies J, Stein R (1998) New aspects of organic carbon deposition and its paleoceanographic implications along the Northern Barents Sea Margin during the last 30,000 years. Paleoceanography 13:384–394. doi:10.1029/98PA01501

Knies J, Vogt C, Stein R (1999) Late Quaternary growth and decay of the Svalbard/Barents Sea ice sheet and paleoceanographic evolution in the adjacent Arctic Ocean. Geo-Mar Lett 18:195–202. doi:10.1007/s003670050068

Knies J, Kleiber H-P, Matthiessen J, Müller C, Nowaczyk N (2001) Marine ice-rafted debris records constrain maximum extent of Saalian and Weichselian ice-sheets along the northern Eurasian margin. Glob Planet Chang 31:45–64. doi:10.1016/s0921-8181(01)00112-6

Koç N, Klitgaard-Kristensen D, Hasle K, Forsberg CF, Solheim A (2002) Late glacial palaeoceanography of Hinlopen Strait, northern Svalbard. Polar Res 21:307–314. doi:10.1111/j.1751-8369.2002.tb00085.x

Kristensen DK, Rasmussen TL, Koç N (2013) Palaeoceanographic changes in the northern Barents Sea during the last 16 000 years – new constraints on the last deglaciation of the Svalbard–Barents Sea Ice Sheet. Boreas 42:798–813. doi:10.1111/j.1502-3885.2012.00307.x

Krögel F, Flemming BW (1998) Evidence for temperature-adjusted sediment distributions in the backbarrier tidal flats of the East Frisian Wadden Sea (southern North Sea). In: Alexander CR, Davis RA, Henry VJ (eds) Tidalites: Processes & products. SEPM Spec Publ 61:31–41

Kuijpers A, Troelstra SR, Prins MA, Linthout K, Akhmetzhanov A, Bouryak S, Bachmann MF, Lassen S, Rasmussen S, Jensen JB (2003) Late Quaternary sedimentary processes and ocean circulation changes at the Southeast Greenland margin. Mar Geol 195:109–129. doi:10.1016/S0025-3227(02)00684-9

Lau YL (1994) Temperature effect on settling velocity and deposition of cohesive sediments. J Hydraul Res 32:41–51. doi:10.1080/00221689409498788

Lisiecki LE, Raymo ME (2005) A Pliocene-Pleistocene stack of 57 globally distributed benthic δ^{18}O records. Paleoceanography 20, PA1003. doi:10.1029/2004PA001071

Lloyd JM, Kroon D, Boulton GS, Laban C, Fallick A (1996) Ice rafting history from the Spitsbergen ice cap over the last 200 kyr. Mar Geol 131:103–121. doi:10.1016/0025-3227(95)00146-8

Lucchi RG, Camerlenghi A, Rebesco M, Colmenero-Hidalgo E, Sierro FJ, Sagnotti L, Urgeles R, Melis R, Morigi C, Bárcena M-A, Giorgetti G, Villa G, Persico D, Flores J-A, Rigual-Hernández AS, Pedrosa MT, Macri P, Caburlotto A (2013) Postglacial sedimentary processes on the Storfjorden and Kveithola trough mouth fans: significance of extreme glacimarine sedimentation. Glob Planet Chang 111:309–326. doi:10.1016/j.gloplacha.2013.10.008

Marshall N, Piper D, Saint-Ange F, Campbell D (2014) Late Quaternary history of contourite drifts and variations in Labrador Current flow, Flemish Pass, offshore eastern Canada. Geo-Mar Lett 34:457–470. doi:10.1007/s00367-014-0377-z

Martinson DG, Pisias NG, Hays JD, Imbrie J, Moore TC, Shackleton NJ (1987) Age dating and the orbital theory of the ice ages: development of a high-resolution 0 to 300,000-year chronostratigraphy. Quat Res 27:1–29. doi:10.1016/0033-5894(87)90046-9

McCave IN, Hall IR (2006) Size sorting in marine muds: processes, pitfalls, and prospects for paleoflow-speed proxies. Geochem Geophys Geosyst 7, Q10N05. doi:10.1029/2006GC001284

McCave IN, Manighetti B, Robinson SG (1996) Sortable silt and fine sediment size/composition slicing: parameters for palaeocurrent speed and palaeoceanography. Paleoceanography 10(3):593–610. doi:10.1029/94PA03039

McCave IN, Crowhurst SJ, Kuhn G, Hillenbrand C-D, Meredith MP (2014) Minimal change in Antarctic Circumpolar Current flow speed between the last glacial and Holocene. Nat Geosci 7:113–116. doi:10.1038/ngeo2037

Meyers PA (1994) Preservation of elemental and isotopic source identification of sedimentary organic matter. Chem Geol 114:289–302. doi:10.1016/0009-2541(94)90059-0

Mulder T, Hassan R, Ducassou E, Zaragosi S, Gonthier E, Hanquiez V, Marchès E, Toucanne S (2013) Contourites in the Gulf of Cadiz: a cautionary note on potentially ambiguous indicators of bottom current activity. Geo-Mar Lett 33(5):357–367. doi:10.1007/s00367-013-0332-4

Müller PJ, Suess E (1979) Productivity, sedimentation rate, and sedimentary organic matter in the oceans—I. Organic carbon preservation. Deep-Sea Res 26A:1347–1362. doi:10.1016/0198-0149(79)90003-7

Noormets R, Hogan K, Austin W, Chauhan T, Roy S, Rasmussen T, Dowdeswell J (2012) Submarine glacial landform assemblages on the outer continental shelf north of Nordaustlandet, Svalbard. In: Abstr Vol 6th Arctic Paleoclimate and Its Extremes (APEX) Meeting, Oulu University, Oululanka Research Station, Finland, 2012, p 70

Nørgaard-Pedersen N (1997) Late Quaternary Arctic Ocean sediment records: surface ocean conditions and provenance of ice-rafted debris. Internal report, Research Centre for Marine Geosciences, Kiel, Germany

Pados T, Spielhagen RF (2014) Species distribution and depth habitat of recent planktic foraminifera in Fram Strait, Arctic Ocean. Polar Res 33:22483. doi:10.3402/polar.v33.22483

Philip GM, Watson DF (1988) Angles measure compositional differences. Geology 16:976–979. doi:10.1130/0091-7613(1988)016<0976:AMCD>2.3.CO;2

Polyak L, Mikhailov V (1996) Post-glacial environments of the southeastern Barents Sea: foraminiferal evidence. Geol Soc Lond Spec Publ 111:323–337

Prins MA, Bouwer LM, Beets CJ, Troelstra SR, Weltje GJ, Kruk RW, Kuijpers A, Vroon PZ (2002) Ocean circulation and iceberg discharge in the glacial North Atlantic: inferences from unmixing of sediment size distributions. Geology 30:555–558. doi:10.1130/0091-7613(2002)030<0555:OCAIDI>2.0.CO;2

Raiswell R, Berner RA (1985) Pyrite formation in euxinic and semi-euxinic sediments. Am J Sci 285(8):710–724. doi:10.2475/ajs.285.8.710

Rasmussen TL, Thomsen E, Nielsen T (2014a) Water mass exchange between the Nordic seas and the Arctic Ocean on millennial time-scale during MIS 4–MIS 2. Geochem Geophys Geosyst 15:530–544. doi:10.1002/2013GC005020

Rasmussen TL, Thomsen E, Skirbekk K, Ślubowska-Woldengen M, Klitgaard DK, Koç N (2014b) Spatial and temporal distribution of Holocene temperature maxima in the northern Nordic seas: interplay of Atlantic-, Arctic- and polar water masses. Quat Sci Rev 92:280–291. doi:10.1016/j.quascirev.2013.10.034

Rebesco M, Wåhlin A, Laberg JS, Schauer U, Beszczynska-Möller A, Lucchi RG, Noormets R, Accettella D, Zarayskaya Y, Diviacco P (2013) Quaternary contourite drifts of the Western Spitsbergen margin. Deep-Sea Res I Oceanogr Res Pap 79:156–168. doi:10.1016/j.dsr.2013.05.013

Rebesco M, Hernández-Molina FJ, Van Rooij D, Wåhlin A (2014) Contourites and associated sediments controlled by deep-water circulation processes: state-of-the-art and future considerations. Mar Geol 352:111–154. doi:10.1016/j.margeo.2014.03.011

Rippeth TP, Lincoln BJ, Lenn Y-D, Green JAM, Sundfjord A, Bacon S (2015) Tide-mediated warming of Arctic halocline by Atlantic heat fluxes over rough topography. Nat Geosci 8:191–194. doi:10.1038/ngeo2350

Rodehacke CB, Hellmer HH, Huhn O, Beckmann A (2007) Ocean/ice shelf interaction in the southern Weddell Sea: results of a regional numerical helium/neon simulation. Ocean Dyn 57:1–11. doi:10.1007/s10236-006-0073-2

Rudels B, Anderson L, Eriksson P, Fahrback E, Jakobsson M, Jones EP, Melling H, Prinsenberg S, Schauer U, Yao T (2012) Observations in the ocean. In: Lemke P, Jacobi H-W (eds) Arctic climate change: the ACSYS decade and beyond. Springer, Berlin, pp 117–198

Rüther DC, Bjarnadóttir LR, Junttila J, Husum K, Rasmussen TL, Lucchi RG, Andreassen K (2012) Pattern and timing of the northwestern Barents Sea Ice Sheet deglaciation and indications of episodic Holocene deposition. Boreas 41(3):494–512. doi:10.1111/j.1502-3885.2011.00244.x

Sarkar S, Berndt C, Chabert A, Masson DG, Minshull TA, Westbrook GK (2011) Switching of a paleo-ice stream in northwest Svalbard. Quat Sci Rev 30:1710–1725. doi:10.1016/j.quascirev.2011.03.013

Schauer U, Fahrbach E, Osterhus S, Rohardt G (2004) Arctic warming through the Fram Strait: oceanic heat transport from 3 years of measurements. J Geophys Res Oceans 109, C06026. doi:10.1029/2003JC001823

Slubowska MA, Koç N, Rasmussen TL, Klitgaard-Kristensen D (2005) Changes in the flow of Atlantic water into the Arctic Ocean since the last deglaciation: evidence from the northern Svalbard continental margin, 80°N. Paleoceanography 20, PA4014. doi:10.1029/2005PA001141

Spielhagen RF, Baumann K-H, Erlenkeuser H, Nowaczyk NR, Nørgaard-Pedersen N, Vogt C, Weiel D (2004) Arctic Ocean deep-sea record of northern Eurasian ice sheet history. Quat Sci Rev 23:1455–1483. doi:10.1016/j.quascirev.2003.12.015

Sternal B, Szczucinski W, Forwick M, Zajaczkowski M, Lorenc S, Przytarska J (2014) Postglacial variability in near-bottom current speed on the continental shelf off south-west Spitsbergen. J Quat Sci 29:767–777. doi:10.1002/jqs.2748

Svendsen JI, Alexanderson H, Astakhov VI, Demidov I, Dowdeswell JA, Funder S, Gataullin V, Henriksen M, Hjort C, Houmark-Nielsen M, Hubberten HW, Ingólfsson Ó, Jakobsson M, Kjær KH, Larsen E, Lokrantz H, Lunkka JP, Lyså A, Mangerud J, Matiouchkov A,

Murray A, Möller P, Niessen F, Nikolskaya O, Polyak L, Saarnisto M, Siegert C, Siegert MJ, Spielhagen R, Stein R (2004) Late Quaternary ice sheet history of northern Eurasia. Quat Sci Rev 23: 1229–1271. doi:10.1016/j.quascirev.2003.12.008

Vogt PR, Crane K, Sundvor E (1994) Deep Pleistocene iceberg plowmarks on the Yermak Plateau: sidescan and 3.5 kHz evidence for thick calving ice fronts and a possible marine ice sheet in the Arctic Ocean. Geology 22:403–406. doi:10.1130/0091-7613(1994)022<0403:DPIPOT>2.3.CO;2

Vogt C, Knies J, Spielhagen RF, Stein R (2001) Detailed mineralogical evidence for two nearly identical glacial/deglacial cycles and Atlantic water advection to the Arctic Ocean during the last 90, 000 years. Glob Planet Chang 31:23–44. doi:10.1016/s0921-8181(01)00111-4

Weaver AJ, Saenko OA, Clark PU, Mitrovica JX (2003) Meltwater pulse 1A from Antarctica as a trigger of the Bølling-Allerød warm interval. Science 299:1709–1713. doi:10.1126/science.1081002

Weltje GJ (1997) End-member modeling of compositional data: numerical-statistical algorithms for solving the explicit mixing problem. Math Geol 29:503–549. doi:10.1007/BF02775085

Wollenburg JE, Kuhnt W, Mackensen A (2001) Changes in Arctic Ocean paleoproductivity and hydrography during the last 145 kyr: the benthic foraminiferal record. Paleoceanography 16:65–77. doi:10.1029/1999PA000454